Beam Size Reconstruction from Ionization Profile Monitors

V. Shiltsev
Fermilab, PO Box 500, MS339, Batavia, IL 60510,USA
(Dated: March 26, 2020)

Ionization profile monitors (IPMs) are widely used in particle accelerators for fast diagnostics of high energy beams. Due to the space-charge effects and several other physical reasons, as well as due to instrumental effects, the measured IPM profiles can significantly differ from those of the beams. There are several empirical mathematical models commonly used for reconstruction of the beam profiles. Here we present a proper correction algorithm based on the space-charge dynamics of the secondaries in IPMs. We also demonstrate the efficiency of the proposed beam size reconstruction algorithm from experimentally measured profiles and discuss practical aspects limiting the IPM accuracy.

I. INTRODUCTION

Ionization profile monitors (IPMs) have been in active use in particle accelerators since late 1960s [1–7] and are important beam diagnostic tools for many modern and future accelerators [8, 9]. Their principle of operation is based on collection of the products of ionization of residual gas by high energy charged particle beams - see detailed discussions and examples of operational instruments in Refs.[10, 11]. Transverse profiles of the secondaries give a very good approximation of the primary beam properties and usually can be quickly measured either on a turn-by-turn or even on a bunch-by-bunch basis. The two most common types of IPMs are distinguished by the use or no-use of a guiding magnetic field parallel to extracting electric field. Physics principles, advantages and disadvantages of the IPMs with a magnetic field are discussed in [12]. This paper deals mostly with the physics principles and beam profile reconstruction in the IPMs operating with only an electric guiding field - those are used more widely because of no-need of external magnets and, therefore, smaller size, simpler design and lower cost (see Fig.1).

One of the key challenges for the initial beam profile reconstruction is proper accounting of various effects which lead to distortion, most often - size expansion - of the charge distribution of secondaries on their travel to the detector and in the detector itself. in high-intensity accelerators, the dominant effect is the increase of the measured beam size σ_m compared to the initial beam size σ_0 caused by space-charge forces of the primary beam. There is an extensive literature on this effect; many simulation codes are developed, presented and discussed in, e.g., proceedings of recent Workshops [13, 14]. Several empirical mathematical models were proposed to relate σ_m and σ_0, such as - from [2]:

$$\sigma_m = \sqrt{\sigma_0^2 + C_1 \frac{N}{E_0 \sigma_0^{1/2}}} \ , \qquad (1)$$

or, alternatively, from [15]:

$$\sigma_m = \sigma_0 + C_2 \frac{N^{1.025}}{\sigma_0^{1.65}} (1 + 1.5R^{1.45})^{-0.28} \ , \qquad (2)$$

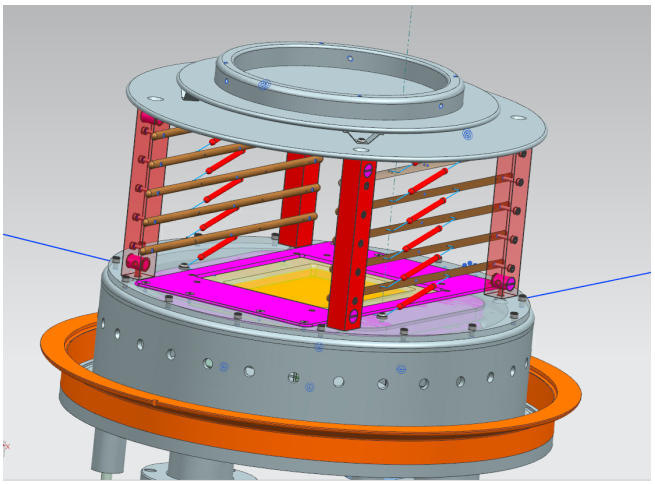

FIG. 1. Fermilab Booster IPM. Proton beam goes from left to right through a 103 mm high HV cage. The maximum voltage on the upper plate is +24 kV, the electric field uniformity is arranged by six-stage voltage divider bars. Secondary ions are accelerated toward a 80×100 mm^2 micro-channel plate (MCP, shown in gold). Electrons, exiting from the MCP, proceed for another 7.5 mm to an array of parallel thin anode strips at +100V above the exit of the MCP, and spaced 1.5 mm apart (not shown) where they are collected and amplified for further processing (courtesy R.Thurman-Keup).

or, from [16]:

$$\sigma_m = \sigma_0 + C_3 \frac{N}{\sigma_0^{0.615}} \ , \qquad (3)$$

here, N is the number of particles in the high energy primary beam, $E_0 = V_0/D$ is the guiding electric field due to the voltage gradient v_0 across the IPM gap D, R is the aspect ratio of (other plane)/(measured plane), e.g., $R_y = \sigma_{0,x}/\sigma_{0,y}$ for vertical plane, and C_1, C_2, C_3 are the constants derived to fit available simulations and measurements data.

Despite acceptable data approximation, such a variety of mathematical constructs, unclear physical reasons for various exponents in Eqs.(1 - 3) and, therefore, undefined applicability ranges, are generally confusing and call for either a better analysis or more sophisticated machine–

This manuscript has been authored by Fermi Research Alliance, LLC under Contract No. DE-AC02-07CH11359 with the U.S. Department of Energy, Office of Science, Office of High Energy Physics.

learning beam profile reconstruction algorithms [17].

Below we develop a new algorithm, based on a well defined physics description and analysis that results in a complete understanding of the IPM signal dependencies on all major parameters, such as high-energy beam intensity N and size σ_0, on the IPM voltage V_0 and dimensions, etc. Moreover, we propose a simple and fast method for inverse calculation of the sought-for beam size σ_0 from the measured size of the IPM profile σ_m, that can be used for online operational processing.

II. SPACE-CHARGE DRIVEN IPM PROFILE EXPANSION

The general equations of transverse motion of the charged secondary particles (ions, electrons) born in the IPM in the acts of ionization of the residual gas molecules are

$$\begin{aligned} \frac{d^2x(t)}{dt^2} &= f_x(r,t)x \\ \frac{d^2y(t)}{dt^2} &= \frac{Ze}{M}E_y + f_y(r,t)y \ , \end{aligned} \tag{4}$$

where Ze and M are charge and mass of the secondaries, $r = \sqrt{x^2+y^2}$, $E_y = V_0/D$ is the IPM extracting external electric field which is assumed to be generated by application of high voltage V_0 over the gap D, and functions $f_{(x,y)}(r,t) = -(Ze/M)\cdot\partial^2U(r,t)/\partial(x,y)^2$ reflect the space-charge impact of the primary high energy particle beam. The space-charge potential $U(x,y)$ is proportional to beam current $J(t)$ and depends on the beam density distribution. For a typical beam in accelerator it scales as $\propto r^2$ at distances less than a characteristic beam size a and as $\propto\ln(r)$ for $r \gg a$, as schematically shown in Fig.2.

For initial analysis we omit complications due to the field distortions at boundaries (such as grounded potential at the MCP plane), assume DC beam current J and for the simplest case of uniform beam with radius a one gets:

$$\begin{aligned} U(x,y) &= -U_{SC}\frac{r^2}{a^2} \quad \text{for } r < a \\ &= -U_{SC}(1+2\ln(r/a)) \quad \text{for } r \geq a \end{aligned} \tag{5}$$

where U_{SC} [V]=$30J$[A]$/\beta_p$, $\beta_p = v_p/c$, v_p the main (proton) beam velocity, and c is the speed of light. The analysis can be further simplified by taking into account that not only the space-charge potential $O(10$ V$)$ is usually small compared to O(10-100 kV) IPM voltage $U_{CS} \ll V_0$, but its gradient $\sim U_{SC}/a$ which is $O(10$ V/mm$)$ in its peak at the edge of the beam is alos small compared to the uniform IPM electric field E_y that is $O(100$ V/mm$)$. In this case, the equation of motion in the y-plane becomes trivial:

$$y(t) = \frac{ZeE_y}{2M}t^2 + v_{0,y}t + y_0 \ , \tag{6}$$

where y_0 and $v_{0,y}$ are the original position and velocity of the secondary particle at the moment of its creation. Combination of the last three equations makes the equation of motion in the plane of expansion as

$$\frac{d^2x(t)}{dt^2} = \frac{x}{\tau_1^2} \ , \tag{7}$$

for particle trajectories inside the high energy beam $r(t) < a$, while outside the high energy beam $r(t) \geq a$ it is:

$$\frac{d^2x(t)}{dt^2} = \frac{x}{\tau_1^2}\frac{a^2}{y(t)^2+x(t)^2} \ . \tag{8}$$

Here we introduced a characteristic expansion time due to the space-charge:

$$\tau_1 = \left(\frac{2eZU_{SC}}{Ma^2}\right)^{-1/2} \ . \tag{9}$$

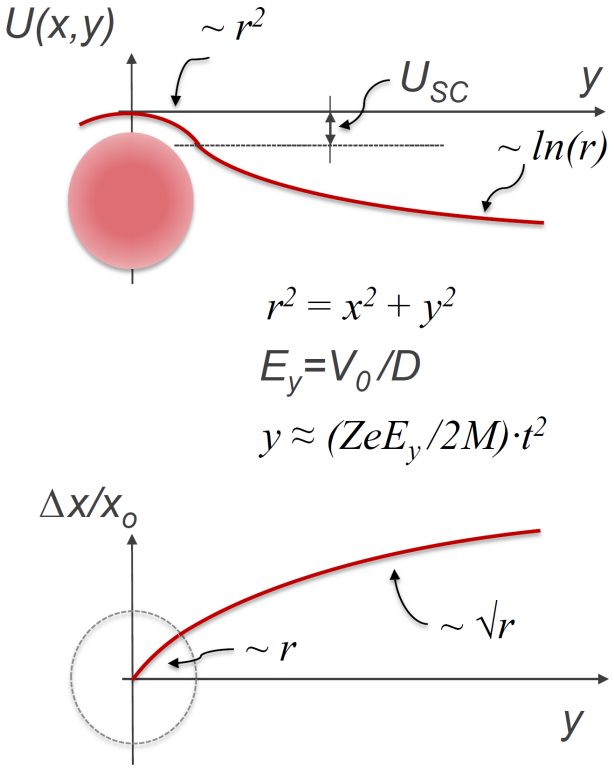

FIG. 2. Proton beam space-charge effect in IPM: (top) the space-charge potential; (bottom) space-charge driven expansion in x-plane in presence of much stronger IPM extraction field E_y (see text).

Solutions of both. Eqs.(7) and (8) are *exponential* functions:

$$x(t) = x_0 \exp h(t) + v_{0,x}t \ . \tag{10}$$

For an initial approximation one can assume that the initial kinetic energy of the secondary particles $\mathcal{E}_i = Mv_0^2/2$

is small compared to eV_0 and eU_{SC} (see more in the next section). Together with the smallness of the initial coordinates compared to the average distance d from the beam center to the MCP plate $(x_0, y_0) \ll d \approx D/2$, one gets for $r(t) < a$:

$$h(t) = \ln\big(\mathrm{ch}(t/\tau_1)\big) \approx \frac{t^2}{2\tau_1^2}\,. \tag{11}$$

After the secondary particle gets out the beam, that is at $r \approx y(t) \geq a$ or $t > \tau_0 \approx \sqrt{2MaD/ZeV_0}$, the solution can be found by stitching the solution Eq.(11) at the beam boundary with exact solution of Eq.(8) with the small term $x^2(t) \ll y^2(t)$ neglected in the denominator:

$$h(t) \approx \frac{\tau_0^2}{\tau_1^2}\Big[\frac{4}{3}\frac{t}{\tau_0} - \frac{5}{6}\Big]\,,\ t > \tau_0. \tag{12}$$

We can note here that the exponential expansion assumes positive right-hand sides in Eqs.(7) and (8), i.e., repulsive nature of the space-charge forces such as for positive ions born in a proton beam or ionization electrons in an electron beam. Of course, a similar analysis can be carried out for the case of attraction and equivalent equations can be derived based on trigonometric (rather than hyperbolic) functions over the same argument of t/τ_1.

At the time when the secondary particle reaches the MCP $\tau_2 \approx \sqrt{2MdD/ZeV_0}$, its transverse position becomes

$$x(\tau_2) \approx x_0 \cdot \exp\Big(\frac{U_{SC}D}{V_0 a} \cdot \Big[\frac{4}{3}\sqrt{\frac{d}{a}} - \frac{5}{6}\Big]\Big)\,. \tag{13}$$

- see Fig.2. It is remarkable that the space-charge expansion is determined only by the space-charge potential U_{SC}, the primary beam size a, the IPM voltage and gap V_0, D and the beam-to-MCP distance d but *does not depend on the type secondary species* (their mass and charge, etc). The basic reason is that both the space-charge impact along x-axis and the transport mechanism along y-axis are set by electric fields. That condition would not hold if, for example, the particle has significant initial velocity $v_{0,y}$ and the second term dominates in the right-hand side of Eq.(6).

Even more remarkable is that the transformation Eq.(13) is linear with respect to x_0 and correspondingly leads to *proportional magnification of the profile* of the distribution of the secondary particles. That allows a relatively straightforward determination of the initial rms beam size σ_0 from the rms size of the IPM profile measured at the MCP σ_m if U_{SC}, V_0, D and d are known.

III. BEAM SIZE RECONSTRUCTION

For a majority of practical IPM applications, the most important outcome is the knowledge of the rms sizes of high energy beams with 5-10% accuracy on a turn-by-turn or comparable time scale. That would correspond to about 10-20% error in the beam emittances - a level comparable with capabilities of other, usually much slower types of beam size diagnostics which then can be used for cross–calibration [8, 18–20]. As we will see below, the space-charge expansion with a typical exponent $h(\tau_2) = 0.1 - 1$ is the largest, though not the only one, of the systematic IPM errors and needs to be known and accounted for with 10-20% accuracy. The most important effects to be taken into account in that regard are: a) a realistic initial distribution of the secondaries which is typically closer to Gaussian with rms size σ_0 then to the uniform one; b) non-round beam with an aspect ratio R significantly different from 1; c) the time structure of the high-energy beam current $J(t)$, especially with high bunching factor $B = J_{peak}/J_{avg}$. Below we will address for these and other effects in order of practical importance.

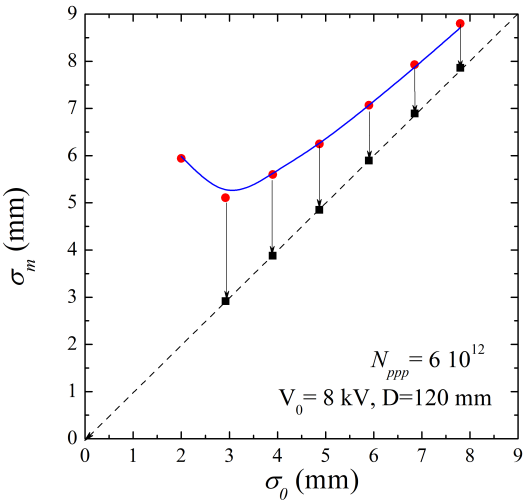

FIG. 3. Vertical rms size of the proton beam profile as measured by an IPM (vertical axis) versus actual size for the parameters $N_p = 6\cdot10^{12}$, $V_0 = 8$kV, $D = 120$mm. Red points are for the Fermilab Booster IPM simulations Ref. [16], blue line is theoretical predication of this paper Eq.(14) with fitting parameters per Eq.(15), and black points are results of the reversion algorithm, i.e., finding the original size σ_0 from the observed one σ_m and the known beam intensity and the IPM parameters, developed in this paper (see also in the text). Dashed diagonal line represents an ideal reconstruction of the rms beam size.

First of all, we extend the parametric dependence of the expansion Eq.(13) to Gaussian beams by using similar relation for the rms size σ_m of the measured profile at the IPM MCP :

$$\sigma_m = \sigma_0 e^{h(U_{SC},\sigma_0,V_0,D)} = \sigma_0 \cdot \exp\Big(\alpha\frac{U_{SC}}{V_0}\Big(\frac{D}{\sigma_0}\Big)^{3/2}\Big)\,. \tag{14}$$

Here we have simplified the expression by taking into account that usually $d \approx D/2$ (beam goes approximately through the IPM center) and dropping the second term in square brackets in Eqs.(12) and (13). The latter is natural for a typical situation of $d \gg a, \sigma_0$ and, therefore, $\tau_2 \gg \tau_0$. For example, for H_2^+ ions in the Fermilab

Booster RCS $\tau_2 \sim 100$ ns $\tau_0 \sim 20$ ns. In any case, all minor deviations can be concealed by a proper choice of the coefficient α.

Calculation of the constant α from the first principles is quite cumbersome. Instead, it can be quite precisely determined from the results of computer simulations of the dynamics of secondaries (ions) in an IPM. Ref.[16] provides an appropriate collection of 104 computer tracking simulations results with 8 values of σ_0 from 2 to 8 mm and 13 values of the total intensity N from 0 to $6{\cdot}10^{12}$ protons circulating in the 475 m circumference Fermilab Booster. The corresponding space-charge potential is $U_{SC} = 18.3$V for the maximum intensity. The IPM gap is D=120 mm and voltage V_0=8 kV. The model (14) with fitting parameter $\alpha = 2.67$ gives an excellent $O(3\%)$agreement with all the simulations of $\sigma_m(N, \sigma_0)$, so the exponent in Eq.(14) can be expressed as:

$$h(N, \sigma_0) = 2.67 \cdot \Big(\frac{N}{6 \cdot 10^{12}}\Big)\Big(\frac{D}{120\,\sigma_0}\Big)^{3/2}\Big(\frac{8\text{kV}}{V_0}\Big)\,. \quad (15)$$

The blue line and red dots in Fig.3 represent this model and the simulations results, respectively.

Now, it is important to have an algorithm to reverse the equation $\sigma_m = \sigma_0 e^{h(N,\sigma_0,V_0,D)}$, i.e., to obtain the original σ_0 from the measured σ_m. One possibility is to modify Eq.(14) to:

$$y = x\,\exp(-x)\,, \quad (16)$$

where

$$x = \frac{3}{2}h = \frac{3}{2}\frac{F}{\sigma_0^{3/3}}, \quad y = \frac{3}{2}\frac{F}{\sigma_m^{3/3}},$$

and F is the factor containing all the constants and parameters other than σ_0 in Eq.(15). The function $y(x)$ is presented in Fig.4. It can be reversed on any of its monotonic ranges using appropriate functions with any desired accuracy. For example, the most relevant to our analysis is the range of $0 < x \leq 1$ that corresponds to maximum $h \leq 2/3$ and the beam size expansion $e^h \leq 2$, where one can use a simple approximation:

$$x = f(y) \approx y\exp\Big(\frac{y}{1 - 3\,y^{5/3}}\Big)\,, \quad (17)$$

Fig.3 illustrates an excellent, within 5%, accuracy of reconstruction of $\sigma_0 =$ (black squares) from the rms IPM profile size σ_m found in the Fermilab Booster simulations [16] using Eqs. (17), (16) and (15). The effect of the high energy beam size aspect ratio R is numerically studied in Ref.[15] and found to be relatively weak, e.g., the corresponding correction of the numerical factor α in Eq.(14) is 1.14 for $R = 0.5$ and 0.84 for $R = 2.0$. If the aimed accuracy of the beam size reconstruction is ∼10%, that factor can be safely neglected for most common cases of h=0.1-1. It should be introduced only if the IPM profile expansion is significant $h > 1$.

The effect of the beam current time structure, such as bunching, depends on the rms bunch length τ_b and time

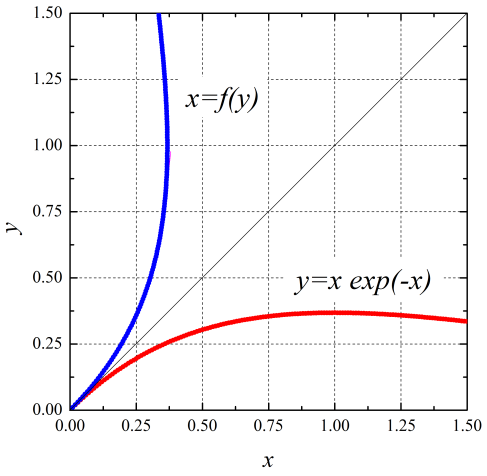

FIG. 4. Illustration on reversion of the IPM beam size equation (see text).

between bunches t_b. In most common cases $\tau_b \ll t_b \lesssim \tau_0 \ll (\tau_1, \tau_2)$ and the dynamics of the cloud of secondary particles in IPM is a sequence of frequent kicks instead of smooth functions as in Eqs. ((4, 7), (8). For example, in the Fermilab Booster $\tau_b \approx 2 - 3$ns, $t_b = 25 - 19ns$, $\tau_0 \approx 20$ ns, $\tau_1 \approx 50ns$ and $\tau_2 \approx 100$ns. In that case our algorithm, based on integration rather than summation, is sufficiently accurate to the level of $O(t_b/\tau_2)$ and Eqs.(14 - 17) are valid. Of course, these equations are also applicable in the case of very long bunches $\tau_b \gg \tau_2$.

Most significant deviations from the above analysis will take place in the case of short and rare bunches $\tau_b \ll (\tau_0, \tau_1, \tau_2) \ll t_b$. In that case, the dynamics of the secondary (ion) is all set by almost instantaneous impact (change in velocity) following the act of ionization, so its position remains unchanged during the passage of the bunch:

$$\Delta v_x = \frac{2ZeN_p}{\beta_p M}\frac{x}{r^2}\Big(1 - \exp(-\frac{r^2}{2\sigma_0^2})\Big)\,, \quad (18)$$

where N_p is the total number of particles in the bunch, which passed by the ion. After this impact, the secondary (ion) sees no transverse field $E_x = 0$ and proceeds to the IPM collector plate under the extracting field E_y. After corresponding time τ_2, the resulting displacement will be $x_0 + \tau_2\Delta v_x$, that is:

$$x(\tau_2) = x_0\Big[1 + 2\kappa\frac{N_p}{r^2}\Big(1 - \exp(-\frac{r^2}{2\sigma_0^2})\Big)\Big]\,, \quad (19)$$

where

$$\kappa = \sqrt{\frac{2eZdD}{M\beta_p^2 V_0}}\,.$$

Averaging over a 2D Gaussian distribution of initial positions and taking into account that on average freshly

generated ions experience the impact of only half of the bunch, one gets the rms size of the IPM profile:

$$\sigma_m^2 = \sigma_0^2 + \kappa N_p + \kappa^2 \frac{N_p^2}{4\sigma_0^2} \ln(2/\sqrt{3}) \,. \qquad (20)$$

Contrary to the case presented in the preceding section and summarized in Eq.(13), the intensity dependent profile expansion of Eq.(20) is not exponential, but rather adds in quadrature and it now depends on charge Z and mass M of the secondary species. In particular, to minimize such expansion in IPMs measuring profiles of short intense and rare bunches, it is beneficial to collect (heavier) ions instead of (light) electrons .

Another effect that calls for the use of ions rather than electrons in IPMs without external magnetic fields is due to the initial velocities of the secondaries v_0. Indeed, assuming such velocities are random with the rms value of $\sqrt{2\mathcal{E}_i/M}$, one gets in quadrature addition to Eq.(14):

$$\sigma_m^2 = \sigma_0^2 e^{2h(U_{SC},\sigma_0,V_0,D)} + \left(\frac{4\mathcal{E}_i dD}{ZeV_0}\right) . \qquad (21)$$

At face value, this additional term is independent of the mass of the secondary particle, but the initial kinetic energy is. For ionization electrons, $\mathcal{E}_i$ is about 35 eV needed on average for ion-electron pair production by protons in hydrogen [21], and, therefore, the corresponding smearing of the particle position measured by the IPM is about $\sigma_T = D\sqrt{2\mathcal{E}_i/ZeV_0}$, that is some 3 mm for voltages as high as $V_0 = 80$ kV and a typical $D = 100$ mm. That is absolutely unacceptable for millimeter or less beam sizes and fast time resolution IPMs that take advantage of short electron reaction time τ_2 must have the external magnetic field B_y to suppress the smearing. As for ions, their the initial kinetic energy is $\sim Z^2 m_e/M$ times smaller and corresponding smearing σ_T is usually well within 0.1 mm.

Other effects leading to intensity independent IPM profile smearing are: a) finite separation Δ between the individual IPM charge collection strips $\sigma_T \simeq \Delta/\sqrt{12}$; b) angular misalignment θ of the long and narrow strips with respect to the high energy beam trajectory $\sigma_T \simeq \theta L$, where L is the strip length; c) charging of dielectric material in between the strips [22] or strip-to-stripe capacitive cross talk; d) non-uniformity of the extraction electric field in the operational IPM aperture $\sigma_T \simeq \sigma_0 |dE_x/dx|/E_y) = \sigma_0 |dE_y/dy|/E_y)$. The latter effect is usually minimized by proper electro-mechanical design.

All the above effects are monitor-specific and the easiest way to account for them is cross-calibration of low intensity beam sizes measured by the IPM σ_m and by another instrument σ^*. In that case, the desired rms instrumental smearing can be found as:

$$\sigma_T^2 = \lim_{N \to 0} \left(\sigma_m^2(N) - \sigma^{*2}(N) \right) . \qquad (22)$$

Fig.5 illustrates the result of such analysis for proton beam profiles measured in the Fermilab Booster cycle

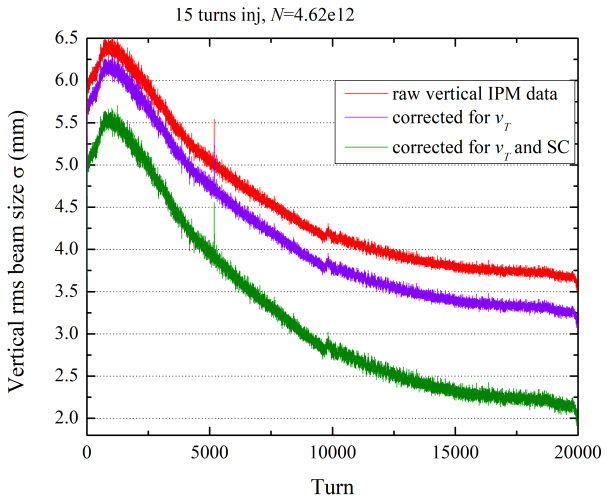

FIG. 5. An example of reconstruction of vertical rms proton beam size in the 33 ms (20000 turns) acceleration cycle of the Fermilab 8 GeV Booster synchtrotron: time dependence of the original IPM data (red), the data corrected for smearing effects (violet) and the same data after additional correction for the space-charge expansion (green).

with $N = 4.62 \cdot 10^{12}$ [20]: the red curve is for the rms vertical beam size $\sigma_m(t)$ as reported by the IPM with $D = 103$ mm and $V_0 = 24$ kV. Separately done comparison with the Booster multi-wire profilometer following Eq.(22) yields $\sigma_T^2 = 2.9$ mm^2. The line in violet in Fig.5 represents the beam size after correction for that error $\sqrt{\sigma_m^2(t) - \sigma_T^2}$. Finally, the true proton rms beam size σ_0 was reconstructed following the algorithm of Eqs. (14 - 17) and is represented by green line. One can see that the overall beam size correction is about 15% early in the Booster acceleration cycle when the rms beam size is about 6 mm. At the end of the cycle, with proton energy increased from 400 MeV to 8 GeV, the correction is almost by a factor of two and accounting for the space-charge expansion is the most important.

IV. CONCLUSIONS

Ionization profile monitors are widely used in various types of particle accelerators for non-intercepting and fast beam profile measurements. As discussed in this paper, the major profile distortions in IPMs are due to expansion of slow ionization secondaries under impact of the space-charge forces of the charged particle beam itself. The distortion is independent on type of collected secondaries (different ions, electrons) and grows with increase of beam intensity N and IPM gap D and decrease of the beam size σ_0 and the IPM extracting voltage V_0 - see Eq.(14). Together with the smearing effect due to significant initial kinetic energy $\mathcal{E}_i$, this precludes operation of IPMs in the electron collection mode unless a

strong external magnetic field is applied along with the IPM electric field. We have developed a model and an algorithm to account for the space-charge expansion in the ion collecting IPMs without an external magnetic field. The rms beam size reconstruction according to Eqs.(15 - 17) allows better than 5-10% accuracy in determination of σ_0 from measured σ_m and known beam intensity and IPM parameters D, V_0 and d (distance from the beam orbit to the IPM MCP plate).

Other, intensity independent instrumental errors σ_T can easily be accounted for in quadrature if the IPM measurements are calibrated against another beam size diagnostics instrument(s) at low beam intensities. The proposed algorithm, though simple and straightforward and addressing the most common operational needs, can not substitute for more sophisticated modeling and analysis if detail knowledge of the high energy beam distribution (shape, tails, etc) is required.

ACKNOWLEDGEMENTS

I would like to thank Jeff Eldred, Valery Kapin, Valery Lebedev, and Kiyomi Seyia for useful discussions, fruitful cooperation and valuable input. I am very grateful to Randy Thurman-Keup for detail description of the operational Fermilab Booster IPMs, for providing Fig.1 and for carefully reading through the manuscript and helpful feedback. Fermi National Accelerator Laboratory is operated by the Fermi Research Alliance, LLC under Contract No. DE-AC02-07CH11359 with the United States Department of Energy..

[1] F. Hornstra and W. DeLuca, in *Proceedings VI Intl. Conf. on High Energy Accel. (Cambridge, MA)* (Sept. 1967) pp. 374–377.
[2] H. Weisberg, E. Gill, P. Ingrassia, and E. Rodger, IEEE Transactions on Nuclear Science **30**, 2179 (1983).
[3] B. Hochadel, F. Albrecht, M. Grieser, D. Habs, D. Schwalm, E. Szmola, and A. Wolf, Nuclear Instruments and Methods in Physics Research Section A: Accelerators, Spectrometers, Detectors and Associated Equipment **343**, 401 (1994).
[4] R. Anne, Y. Georget, R. Hue, C. Tribouillard, and J. L. Vignet, Nuclear Instruments and Methods in Physics Research Section A: Accelerators, Spectrometers, Detectors and Associated Equipment **329**, 21 (1993).
[5] R. Connolly, R. Michnoff, T. Moore, T. Shea, and S. Tepikian, Nuclear Instruments and Methods in Physics Research Section A: Accelerators, Spectrometers, Detectors and Associated Equipment **443**, 215 (2000).
[6] A. Jansson, T. Fitzpatrick, K. Bowie, R. Kwarciany, C. Lundberg, D. Slimmer, L. Valerio, and J. Zagel, in *AIP Conference Proceedings*, Vol. 868 (American Institute of Physics, 2006) pp. 159–167.
[7] S. Levasseur, B. Dehning, S. Gibson, H. Sandberg, M. Sapinski, K. Sato, G. Schneider, and J. Storey, Journal of instrumentation **12**, C02050 (2017).
[8] R. S. Moore, A. Jansson, and V. Shiltsev, Journal of Instrumentation **4**, P12018 (2009).
[9] F. Benedetti, P. Abbon, F. Belloni, G. Coulloux, F. Gougnaud, C. Lahonde-Hamdoun, P. Le Bourlout, Y. Mariette, J. Marroncle, J. Mols, *et al.*, in *EPJ Web of Conferences*, Vol. 225 (EDP Sciences, 2020) p. 01009.
[10] P. Strehl, *Beam instrumentation and diagnostics*, Vol. 120 (Springer, 2006).
[11] K. Wittenburg, arXiv preprint arXiv:1303.6767 (2013).
[12] D. Vilsmeier, M. Sapinski, and R. Singh, Physical Review Accelerators and Beams **22**, 052801 (2019).
[13] Ionisation Profile Monitor Simulation Kickoff Workshop (CERN, March 3-4, 2016), `https://indico.cern.ch/event/491615/`, accessed: March 3, 2020.
[14] Workshop on Simulations, Design and Operational Experience of Ionisation Profile Monitors (GSI, May 21-24, 2017), `https://indico.gsi.de/event/5366/`, accessed: March 3, 2020.
[15] R. Thern, in *1987 IEEE Particle Accelerator Conf.(PAC'87), Washington, DC, 16-19 May 1987* (IEEE, 1987) pp. 646–648.
[16] J. Amundson, J. Lackey, P. Spentzouris, G. Jungman, and L. Spentzouris, Physical Review Special Topics-Accelerators and Beams **6**, 102801 (2003).
[17] D. Vilsmeier, M. Sapinski, R. Singh, and J. Storey, Journal of Physics: Conference Series **1067**, 072003 (2018).
[18] V. Lebedev and V. Shiltsev, eds., *Accelerator physics at the Tevatron collider* (Springer, 2012).
[19] F. Roncarolo, *Accuracy of the transverse emittance measurements of the CERN Large Hadron Collider*, Tech. Rep. (CERN-THESIS-2005-082, 2005).
[20] V.Shiltsev, *On Booster Intensity and IPM Diagnostics*, Fermilab-beams-doc-7997 (unpublished, 2020), `https://beamdocs.fnal.gov/`, accessed: March 18, 2020.
[21] C. Bakker and E. Segre, Physical Review **81**, 489 (1951).
[22] V.Lebedev, private communication, (2020).